Thermal Effects in Binary Neutron Star Mergers

Jacob Fields,[1,2,*] Aviral Prakash,[1,2] Matteo Breschi,[3,4,5] David Radice,[2,1,6,†] Sebastiano Bernuzzi,[3] and André da Silva Schneider[7]

[1]*Department of Physics, The Pennsylvania State University, University Park, PA 16802*
[2]*Institute for Gravitation & the Cosmos, The Pennsylvania State University, University Park, PA 16802*
[3]*Theoretisch-Physikalisches Institut, Friedrich-Schiller-Universität Jena, 07743, Jena, Germany*
[4]*Scuola Internazionale Superiore di Studi Avanzati (SISSA), 34136 Trieste, Italy*
[5]*Istituto Nazionale di Fisica Nucleare (INFN), Sezione di Trieste, 34127 Trieste, Italy*
[6]*Department of Astronomy & Astrophysics, The Pennsylvania State University,University Park, PA 16802*
[7]*Departamento de Física, Universidade Federal de Santa Catarina, Florianópolis, SC 88040-900, Brazil*

(Dated: February 21, 2023)

We study the impact of finite-temperature effects in numerical-relativity simulations of binary neutron star mergers with finite-temperature microphysical equations of state and neutrino transport in which we vary the effective nucleon masses in a controlled way. We find that, as the specific heat is increased, the merger remnants become colder and more compact due to the reduced thermal pressure support. Using a full Bayesian analysis, we demonstrate that this effect will be measurable in the postmerger gravitational wave signal with next-generation observatories at signal-to-noise ratios as low as 10, i.e., close to the detectability threshold of post-merger signals.

Introduction. The extreme conditions found in neutron stars make them an ideal means for probing the nuclear equation of state (EOS). Electromagnetic (EM) observations of pulsars have provided valuable information about the mass distribution of neutron stars [1, 2], and recent results from NICER offer constraints on their radii [3–5]. Binary neutron star (BNS) mergers give additional astronomical constraints; the gravitational waves (GW) and EM counterpart of GW170817 contained details about the EOS via tidal deformability measurements and ejecta characteristics [6–12].

Due to the high Fermi temperature of matter in a neutron star, pulsars and BNS inspirals agree well with a zero-temperature approximation; for BNS systems, this approximation breaks down in the post-merger phase, where hot spots in the outer core may exceed 100 MeV [13]. Consequently, constraints obtained from pulsars and BNS inspirals apply specifically to the cold EOS, while the post-merger phase may contain information about the finite-temperature EOS. Current GW detectors have not yet observed a BNS post-merger [6, 14, 15]. Nevertheless, future detectors, like the proposed Einstein Telescope (ET) [16] and Cosmic Explorer (CE) [17] detectors, will feature improved sensitivity at the higher frequencies necessary to see a BNS post-merger signal, perhaps at signal-to-noise ratios (SNR) as low as 8 [18]. Additionally, sensitivity upgrades to current instruments promise higher BNS detection counts with better sky localization [19].

State-of-the-art BNS merger simulations typically incorporate thermal effects via full finite-temperature EOSs, often in the form of a table [20, 21], and realistic neutrino transport, such as via elaborate moment approximations [22, 23] or Monte Carlo methods [24]. Many studies perform simulations with multiple finite-temperature EOSs to demonstrate sensitivity (or lack thereof, as the case may be) of BNS merger observables under different scenarios, but the different cold-temperature behavior of each EOS makes it difficult to attribute specific outcomes to finite-temperature behavior [8, 13, 25–28]. Others do incorporate various EOS models which differ only in finite-temperature behavior, but only as a comparison between a full EOS table with an approximate method [20, 29, 30]. Only more recently has work become available which examine systematic changes in finite-temperature behavior while keeping the zero-temperature EOS fixed [31]. Furthermore, none of these studies incorporate all the relevant physics, particularly consistent neutrino transport.

In this *Letter*, we present a first GR neutrino-radiation hydrodynamics study of finite-temperature effects of a realistic nuclear EOS on BNS mergers through modifications to the specific heat capacity. Our simulations show that an increased heat capacity results in denser, cooler remnants. This leaves clear imprints on the GW signal in the post-merger phase, which we show can be recovered in a parameter estimation pipeline tuned to a next-generation GW observatory.

Methods. We select three non-relativistic Skyrme-type nucleonic EOSs built with the framework of Ref. [32] which were parameterized to produce the same cold nuclear matter bulk properties but different specific heat content. In the model, the specific heat is controlled by the *temperature-independent* effective masses of neutrons and protons, m_n^* and m_p^*, respectively, which have a simple phenomenological description [32–34]. The effective masses depend on the nucleonic number densities, n_n and n_p (or, alternatively, the number density $n = n_n + n_p$ and the proton fraction $Y_p = n_p/n$ of matter), and converge toward the vacuum nucleon masses at zero density. Furthermore, m_n^* and m_p^* also depend on two parameters which were chosen to reproduce two yet poorly con-

strained nuclear matter observables at saturation density [34]: the effective mass for symmetric nuclear matter, $m^* = m_n^* \simeq m_p^*$, and the difference in the neutron and proton effective masses for pure neutron matter, Δm^*.

The three selected EOSs attribute different values to m^*, $m^*/m_n = \{0.55, 0.75, 0.95\}$, but predict the same $\Delta m^* = 0.10$ and other bulk nuclear matter properties. Further details are discussed in Section 2.2 of Ref. [35], where the same three EOSs were used to study GW signals from core-collapse supernovae, and also [32, 36]. We note that, to first order, the baryonic contribution to the specific heat of the degenerate nuclear matter as found in the core of a neutron star, which dominates over the lepton contribution, is given by $c_v = \left(\frac{\pi}{3}\right)^{2/3} \frac{T}{n} \left(n_p^{1/3} m_p^* + n_n^{1/3} m_n^*\right)$, see Eq. (151) of Ref. [33]. Thus, all else being equal, increasing m^* leads to a larger specific heat capacity for matter in the merger remnant to which we attribute the differences seen across our simulations.

Using the pseudospectral code `LORENE` [37], we construct initial data for equal-mass binary neutron star systems in quasicircular orbit with a gravitational mass of $M = 1.35$ $M_\odot$ per star. We evolve each binary using `THC_M1` [23, 38], an extension of the `THC` numerical relativity code [39, 40] incorporating neutrino transport via a moment formalism [41, 42]. We perform each simulation at two resolutions, designated as `LR` and `SR`, which correspond to a grid spacing in the finest refinement level covering both stars during the inspiral and the merger remnant of $\Delta x \approx 250$ m and $\Delta x \approx 180$ m, respectively, at the finest refinement level. We also run identical `SR` simulations with our older M0 solver [43] to validate our results; though the solver is less accurate and does not properly capture effects such as neutrino trapping, these runs support the major results of the M1 runs.

Results. Figure 1 shows slices of the x-z plane for the $m^* = 0.55$ and $m^* = 0.95$ SR simulations at approximately 5 ms post-merger. Even at this relatively early post-merger time, the density of the remnant is noticeably larger in the $m^* = 0.95$ model. Temperature also appears to decrease; the outer core of the neutron star is noticeably hotter for the $m^* = 0.55$ model. Figure 2, which includes the $m^* = 0.75$ SR data, illustrates that this is a more general trend, where the middle panel shows that the maximum rest-mass density is highest in the $m^* = 0.95$ model and lowest for $m^* = 0.55$ at most post-merger times.

The GW strain in Figure 2 demonstrates identical behavior in the inspiral for all three models, but the waveforms begin to deviate in the post-merger due to finite-temperature effects in the EOS. The differences in morphology include frequency evolution, amplitude, damping times, and modulations. This is more quantitatively seen in the GW spectrum (see Figure 3), where the behavior is qualitatively similar but noticeably different; in particular, there is a clear rightward shift in the peak postmerger frequency, f_2, as m^* increases. Table I contains f_2 for both the LR and SR simulations. Though the precision of the NR waveform is limited by finite resolution and step size, the shift of $\Delta f \gtrsim 10$ Hz is robust across resolutions, which suggests it is an effect of the EOS and not an artifact of the simulations. The M0 SR simulation demonstrates a similar trend, though the $m^* = 0.75$ run is much closer to the $m^* = 0.95$ model than either of the M1 cases. This provides an important sanity check of our results, but we stress that it is only qualitative; the M1 results must be used for quantitative analysis of post-merger effects, as a self-consistent approach which accounts for neutrino trapping noticeably changes the remnant's evolution [38].

To detect these thermal effects in the postmerger via next-generation GW detectors and possibly constrain the m^* nuclear parameter, we perform full Bayesian inference on the postmerger GW signals. To compute injections, we extract the postmerger waveforms from the SR simulations by applying a Tukey window to suppress the inspiral and spline interpolate the GW waveforms to a sampling rate of 16384 Hz. We further zero pad the signals to a segment of 1 s. For brevity, we consider here only noise-less injections. For parameter estimation, we employ the publicly available code `bajes` [44] and use the `UltraNest` [45] sampler available as part of the `bajes` pipeline. We recover the injections by using the postmerger model `NRPMw` from [18] and compute posteriors on its parameters. We inject all signals at a luminosity distance corresponding to an SNR of 10, assuming the power spectral density of ET-D [46] to simulate the detector response. The priors are set in accordance to [47], section-IIB. In Figure 3, we show the reconstructed waveforms from `NRPMw` evaluated on the parameter space of the recovered posterior samples. We list the recovered SNRs and f_2 values in Table I. At SNR = 10, the injected spectrum's f_2 frequencies sit well within the 90% credible intervals of the distribution of reconstructed waveform's f_2 frequencies. Furthermore, these intervals touch but do not overlap, indicating that we can distinguish all three waveforms at SNR = 10 with 90% confidence.

Discussion. We have shown that m^* significantly influences the GW signals in BNS mergers, and we have analyzed this effect in detail for f_2. The relationship between m^* and f_2 is easily explained in terms of the specific heat. Increasing the specific heat appears to soften the equation of state; because it requires more energy to increase the temperature, there is less thermal pressure available to support the star, thus producing a more rapidly rotating and compact remnant with lower temperatures.

The EOSs we use have a simple relationship between m^* and the specific heat capacity which may not be representative of the true nuclear EOS. Nevertheless, this study serves as a proof of concept demonstrating that fu-

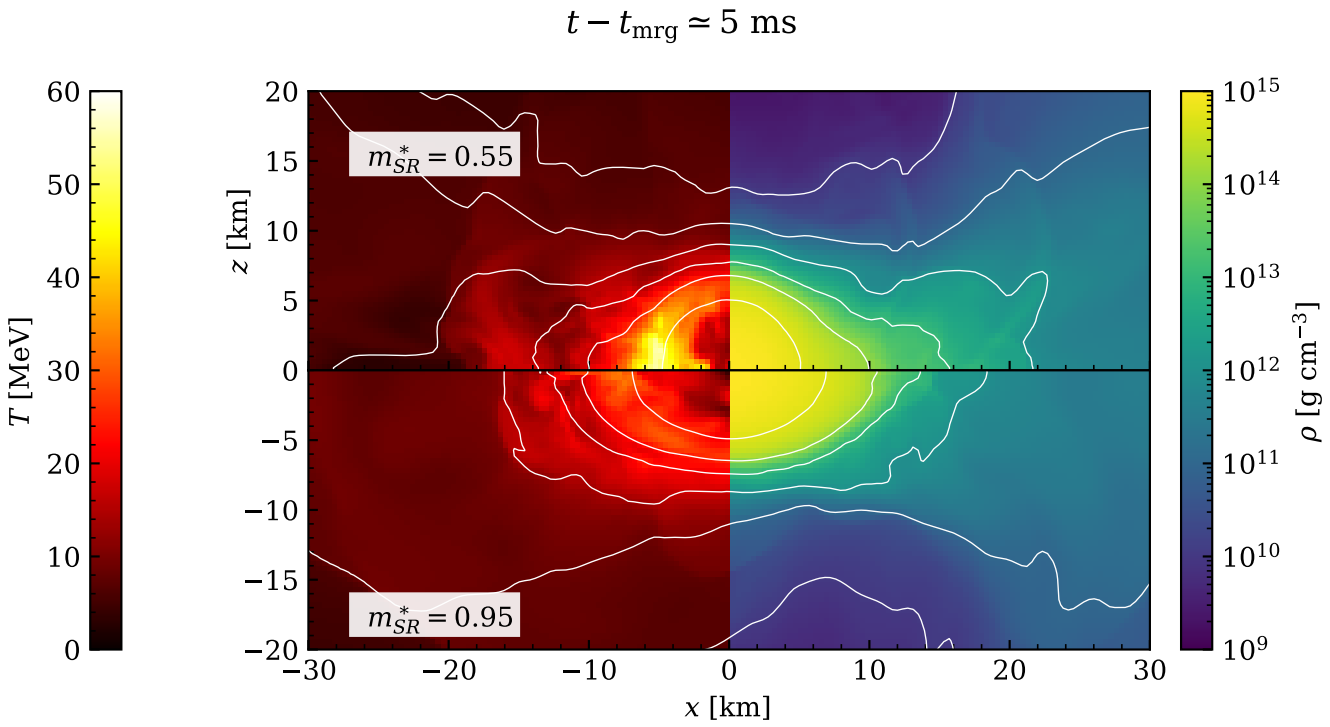

FIG. 1. Temperature and rest-mass density slices in the x-z plane of the $m^* = 0.55$ and $m^* = 0.95$ SR simulations at approximately 5 ms post-merger. Contour lines correspond to rest-mass densities $\rho = \{10^{10}, 10^{11}, 10^{12}, 10^{13}, 10^{14}, 5 \times 10^{14}\}$ g cm^{-3}. For visual clarity, the $m^* = 0.75$ model is not shown.

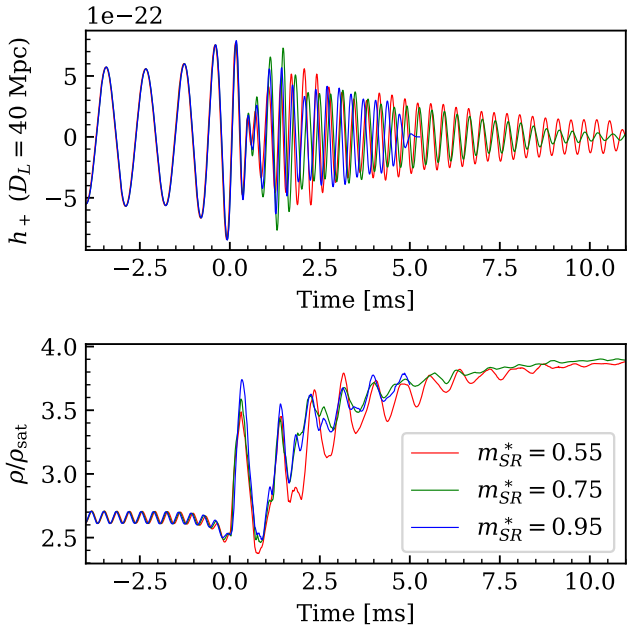

FIG. 2. The gravitational wave strain of the $\ell = 2$, $m = 2$ mode (top) and the maximum rest-mass density of the SR simulations (bottom).

TABLE I. Peak post-merger frequencies (f_2) of the gravitational wave spectrum for each simulation. LR and SR indicate the low-resolution and high-resolution simulations, respectively, and M0 indicates the model run with the M0 solver. The column labeled NRPMw indicates the f_2 of the `NRPMw` model. For reference, the recovered matched-filter SNR values are also listed; each model was injected at SNR = 10. For consistency, all peaks are measured after suppressing the inspiral with a Tukey window function. We also provide the mismatch, $\mathcal{M}$ (see Ref. [48, 49]), between the $f_2^{\rm SR}$ runs, with one column measured against $m^* = 0.75$ and the other against $m^* = 0.95$.

m^* (m_n)	$f_2^{\rm LR}$ (kHz)	$f_2^{\rm SR,M0}$ (kHz)	$f_2^{\rm SR}$ (kHz)	$\mathcal{M}^{\rm SR}_{0.75}$	$\mathcal{M}^{\rm SR}_{0.95}$ (kHz)	$f_2^{\rm NRPMw}$	SNR$_{\rm mf}$
0.55	2.862	2.864	2.835	0.04	0.09	$2.884^{+0.0}_{-0.1}$	$8.98^{+1.14}_{-1.73}$
0.75	2.908	2.966	2.908	N/A	0.08	$2.884^{+0.1}_{-0.0}$	$8.77^{+1.07}_{-1.57}$
0.95	2.921	2.974	3.080	0.08	N/A	$3.084^{+0.0}_{-0.1}$	$8.86^{+1.26}_{-1.54}$

ture detectors like ET and CE can use f_2 to constrain the finite-temperature EOS. We also reiterate that this effect *only* affects the finite-temperature evolution, so it will not be observable until next-generation detectors sensitive to the post-merger phase come online.

We do acknowledge some limitations in our work; most notably, the length of the $m^* = 0.95$ M1 simulations is

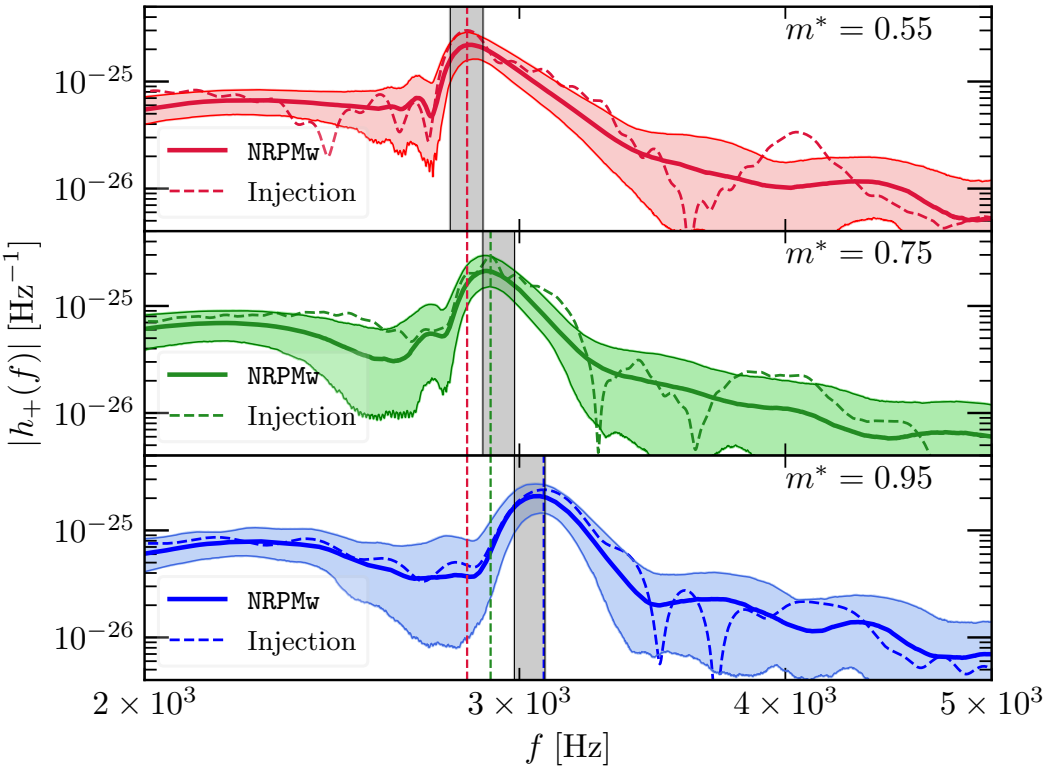

FIG. 3. The reconstructed GW spectrum of the $\ell = 2$, $m = 2$ mode using the NRPMw model. The colored solid lines represent the median waveform and the colored shaded regions represent the 90% credible intervals on the posterior distribution of the spectra computed from the recovered parameter space of NRPMw. The colored dashed limes represent the injected spectra at an SNR of 10. Additionally, shown are the postmerger peak frequencies f_2 (in vertical dashed lines) and the 90% credible intervals (in grey) on the posterior distribution of f_2 from the reconstructed waveforms.

much shorter than both the $m^* = 0.55$ and $m^* = 0.75$ runs due to a limitation in the M1 neutrino solver which introduced unphysical effects past 5 ms post-merger. This short length may explain why $f_2^{m^*=0.95}$ increases between the LR and SR runs while both $f_2^{m^*=0.55}$ and $f_2^{m^*=0.75}$ instead decrease, as a shorter signal will introduce a extra spread of frequencies to the power spectrum and possibly shift the peak.

We may consider several avenues for future work. Longer simulations would allow us to investigate the ejecta and consider possible effects on EM counterparts. Additionally, Zappa *et al.* [38] indicate that resolution has a prominent influence on post-merger evolution, including collapse time and disk formation, suggesting the need for higher resolution runs. To investigate our hypothesis that this study's results are more general, future simulations could also explore other EOS models with tunable finite-temperature behavior.

The authors thank Albino Perego, Ish Gupta, Arnab Dhani, Rahul Kashyap and Bangalore Sathyaprakash for helpful discussions. DR acknowledges funding from the U.S. Department of Energy, Office of Science, Division of Nuclear Physics under Award Number(s) DE-SC0021177 and from the National Science Foundation under Grants No. PHY-2011725, PHY-2020275, PHY-2116686, and AST-2108467. SB acknowledges support by the EU H2020 under ERC Starting Grant, no. BinGraSp-714626 and from the Deutsche Forschungsgemeinschaft DFG project MEMI number BE 6301/2-1. MB acknowledges support by the PRO3 program "DS4Astro" of the Italian Ministry for Universities and Research. Simulations were performed on PSC Bridges2 (NSF XSEDE allocation TG-PHY160025). This research used resources of the National Energy Research Scientific Computing Center, a DOE Office of Science User Facility supported by the Office of Science of the U.S. Department of Energy under Contract No. DE-AC02-05CH11231. Computations for this research were performed on the Pennsylvania State University's Institute for Computational and Data Sciences' Roar supercomputer.

* jmf6719@psu.edu
† Alfred P. Sloan fellow

[1] J. M. Lattimer and M. Prakash, The Astrophysical Jour-

nal **550**, 426 (2001).
[2] J. Alsing, H. O. Silva, and E. Berti, Mon. Not. Roy. Astron. Soc. **478**, 1377 (2018), arXiv:1709.07889 [astro-ph.HE].
[3] T. E. Riley *et al.*, Astrophys. J. Lett. **918**, L27 (2021), arXiv:2105.06980 [astro-ph.HE].
[4] R. M. Ludlam *et al.*, Astrophys. J. **927**, 112 (2022), arXiv:2201.11767 [astro-ph.HE].
[5] T. Salmi *et al.*, Astrophys. J. **941**, 150 (2022), arXiv:2209.12840 [astro-ph.HE].
[6] B. P. Abbott *et al.* (LIGO Scientific Collaboration and Virgo Collaboration), Phys. Rev. Lett. **119**, 161101 (2017).
[7] B. Margalit and B. D. Metzger, Astrophys. J. Lett. **850**, L19 (2017), arXiv:1710.05938 [astro-ph.HE].
[8] D. Radice, A. Perego, F. Zappa, and S. Bernuzzi, Astrophys. J. Lett. **852**, L29 (2018), arXiv:1711.03647 [astro-ph.HE].
[9] S. De, D. Finstad, J. M. Lattimer, D. A. Brown, E. Berger, and C. M. Biwer, Phys. Rev. Lett. **121**, 091102 (2018), [Erratum: Phys.Rev.Lett. 121, 259902 (2018)], arXiv:1804.08583 [astro-ph.HE].
[10] B. P. Abbott *et al.* (LIGO Scientific, Virgo), Phys. Rev. Lett. **121**, 161101 (2018), arXiv:1805.11581 [gr-qc].
[11] T. Dietrich, M. W. Coughlin, P. T. H. Pang, M. Bulla, J. Heinzel, L. Issa, I. Tews, and S. Antier, Science **370**, 1450 (2020), arXiv:2002.11355 [astro-ph.HE].
[12] R. Kashyap *et al.*, Phys. Rev. D **105**, 103022 (2022), arXiv:2111.05183 [astro-ph.HE].
[13] A. Perego, S. Bernuzzi, and D. Radice, Eur. Phys. J. A **55**, 124 (2019).
[14] B. P. Abbott *et al.* (LIGO Scientific Collaboration and Virgo Collaboration), Astrophys. J. Lett. **848**, L12 (2017).
[15] B. P. Abbott *et al.* (LIGO Scientific Collaboration and Virgo Collaboration), Astrophys. J. Lett. **892**, L3 (2020).
[16] M. Maggiore *et al.*, JCAP **2020** (03), 050, arXiv:1912.02622 [astro-ph.CO].
[17] B. P. Abbott *et al.* (LIGO Scientific), Class. Quant. Grav. **34**, 044001 (2017), arXiv:1607.08697 [astro-ph.IM].
[18] M. Breschi, S. Bernuzzi, K. Chakravarti, A. Camilletti, A. Prakash, and A. Perego, (2022), arXiv:2205.09112 [gr-qc].
[19] B. P. Abbott *et al.* (KAGRA, LIGO Scientific, Virgo, VIRGO), Living Rev. Rel. **21**, 3 (2018), arXiv:1304.0670 [gr-qc].
[20] A. Bauswein, H. T. Janka, and R. Oechslin, Phys. Rev. D **82**, 084043 (2010), arXiv:1006.3315 [astro-ph.SR].
[21] Y. Sekiguchi, K. Kiuchi, K. Kyutoku, and M. Shibata, Phys. Rev. Lett. **107**, 051102 (2011), arXiv:1105.2125 [gr-qc].
[22] F. Foucart, E. O'Connor, L. Roberts, L. E. Kidder, H. P. Pfeiffer, and M. A. Scheel, Phys. Rev. D **94**, 123016 (2016), arXiv:1607.07450 [astro-ph.HE].
[23] D. Radice, S. Bernuzzi, A. Perego, and R. Haas, Mon. Not. Roy. Astron. Soc. **512**, 1499 (2022), arXiv:2111.14858 [astro-ph.HE].
[24] F. Foucart, M. D. Duez, R. Haas, L. E. Kidder, H. P. Pfeiffer, M. A. Scheel, and E. Spira-Savett, (2022), arXiv:2210.05670 [astro-ph.HE].
[25] D. Neilsen, S. L. Liebling, M. Anderson, L. Lehner, E. O'Connor, and C. Palenzuela, Phys. Rev. D **89**, 104029 (2014), arXiv:1403.3680 [gr-qc].
[26] E. R. Most, L. J. Papenfort, V. Dexheimer, M. Hanauske, S. Schramm, H. Stöcker, and L. Rezzolla, Phys. Rev. Lett. **122**, 061101 (2019), arXiv:1807.03684 [astro-ph.HE].
[27] P. Hammond, I. Hawke, and N. Andersson, Phys. Rev. D **104**, 103006 (2021), arXiv:2108.08649 [astro-ph.HE].
[28] A. Camilletti, L. Chiesa, G. Ricigliano, A. Perego, L. C. Lippold, S. Padamata, S. Bernuzzi, D. Radice, D. Logoteta, and F. M. Guercilena, Mon. Not. Roy. Astron. Soc. 10.1093/mnras/stac2333 (2022), arXiv:2204.05336 [astro-ph.HE].
[29] .
[30] C. A. Raithel, P. Espino, and V. Paschalidis, Mon. Not. Roy. Astron. Soc. **516**, 4792 (2022), arXiv:2206.14838 [astro-ph.HE].
[31] C. Raithel, V. Paschalidis, and F. Özel, Phys. Rev. D **104**, 063016 (2021), arXiv:2104.07226 [astro-ph.HE].
[32] A. S. Schneider, L. F. Roberts, C. D. Ott, and E. O'Connor, Phys. Rev. C **100**, 055802 (2019).
[33] C. Constantinou, B. Muccioli, M. Prakash, and J. M. Lattimer, Phys. Rev. C **89**, 065802 (2014).
[34] J. Margueron, R. Hoffmann Casali, and F. Gulminelli, Phys. Rev. C **97**, 025805 (2018).
[35] O. E. Andersen, S. Zha, A. da Silva Schneider, A. Betranhandy, S. M. Couch, and E. P. O'Connor, The Astrophysical Journal **923**, 201 (2021).
[36] H. Yasin, S. Schäfer, A. Arcones, and A. Schwenk, Phys. Rev. Lett. **124**, 092701 (2020).
[37] E. Gourgoulhon, P. Grandclément, J.-A. Marck, J. Novak, and K. Taniguchi, LORENE: Spectral methods differential equations solver, Astrophysics Source Code Library, record ascl:1608.018 (2016), ascl:1608.018.
[38] F. Zappa, S. Bernuzzi, D. Radice, and A. Perego, (2022), arXiv:2210.11491 [astro-ph.HE].
[39] D. Radice, L. Rezzolla, and F. Galeazzi, Mon. Not. Roy. Astron. Soc. **437**, L46 (2014), arXiv:1306.6052 [gr-qc].
[40] D. Radice, L. Rezzolla, and F. Galeazzi, Classical and Quantum Gravity **31**, 075012 (2014).
[41] K. S. Thorne, Mon. Not. Roy. Astron. Soc. **194**, 439 (1981).
[42] M. Shibata, K. Kiuchi, Y.-i. Sekiguchi, and Y. Suwa, Prog. Theor. Phys. **125**, 1255 (2011), arXiv:1104.3937 [astro-ph.HE].
[43] D. Radice, F. Galeazzi, J. Lippuner, L. F. Roberts, C. D. Ott, and L. Rezzolla, Mon. Not. Roy. Astron. Soc. **460**, 3255 (2016), arXiv:1601.02426 [astro-ph.HE].
[44] M. Breschi, R. Gamba, and S. Bernuzzi, Phys. Rev. D **104**, 042001 (2021), arXiv:2102.00017 [gr-qc].
[45] J. Buchner, UltraNest - a robust, general purpose Bayesian inference engine (2021).
[46] S. Hild *et al.*, Class. Quant. Grav. **28**, 094013 (2011), arXiv:1012.0908 [gr-qc].
[47] M. Breschi, R. Gamba, S. Borhanian, G. Carullo, and S. Bernuzzi, (2022), arXiv:2205.09979 [gr-qc].
[48] L. Lindblom, B. J. Owen, and D. A. Brown, Phys. Rev. D **78**, 124020 (2008), arXiv:0809.3844 [gr-qc].
[49] T. Damour, A. Nagar, and M. Trias, Phys. Rev. D **83**, 024006 (2011), arXiv:1009.5998 [gr-qc].